J. Fluid Mech. (1999), *vol.* 397, *pp.* 203–229. Printed in the United Kingdom

The effect of boundaries on the plane Couette flow of granular materials: a bifurcation analysis

By P. R. NOTT[1], M. ALAM[1], K. AGRAWAL[2], R. JACKSON[2] AND S. SUNDARESAN[2]

[1] Department of Chemical Engineering, Indian Institute of Science, Bangalore 560012, India

[2] Department of Chemical Engineering, Princeton University, Princeton, NJ 08544, USA

(Received 28 October 1998 and in revised form 20 May 1999)

The tendency of granular materials in rapid shear flow to form non-uniform structures is well documented in the literature. Through a linear stability analysis of the solution of continuum equations for rapid shear flow of a uniform granular material, performed by Savage (1992) and others subsequently, it has been shown that an infinite plane shearing motion may be unstable in the Lyapunov sense, provided the mean volume fraction of particles is above a critical value. This instability leads to the formation of alternating layers of high and low particle concentrations oriented parallel to the plane of shear. Computer simulations, on the other hand, reveal that non-uniform structures are possible even when the mean volume fraction of particles is small. In the present study, we have examined the structure of fully developed layered solutions, by making use of numerical continuation techniques and bifurcation theory. It is shown that the continuum equations do predict the existence of layered solutions of high amplitude even when the uniform state is linearly stable. An analysis of the effect of bounding walls on the bifurcation structure reveals that the nature of the wall boundary conditions plays a pivotal role in selecting that branch of non-uniform solutions which emerges as the primary branch. This demonstrates unequivocally that the results on the stability of bounded shear flow of granular materials presented previously by Wang *et al.* (1996) are, in general, based on erroneous base states.

1. Introduction

The formation of non-uniform structures in rapid granular flows has been observed in many recent experiments and computer simulations (Hopkins & Louge 1991; Savage 1992*a*; Goldhirsch, Tan & Zanetti 1993; Miller, O'Hern & Behringer 1996). As continuum equations of motion, such as those derived from the kinetic theory of granular materials (for example, see Lun *et al.* 1984, and Jenkins & Richman 1985*a*), are commonly used to model such flows, it is of interest to determine whether these structures can be captured by such equations in a qualitatively correct manner.

Mello, Diamond & Levine (1991) examined plane shearing motion using continuum equations derived from granular kinetic theory and investigated the propagation of disturbances with wave vectors in the direction of the vorticity. Instabilities which arise during the cooling of an initially uniform granular material as a result of inelastic collisions have been examined by Goldhirsch *et al.* (1993) and McNamara (1993). The stability of the solution of the continuum equations representing an infinite plane

shearing motion has been examined in detail by Savage (1992*b*) and Babić (1993). They focused on the Kelvin modes, namely disturbances which take the form of wavefronts rotating in conformity with the vorticity of the base-state flow field, and found large initial growth rates. The relation of the Kelvin modes to stability has been clarified by Schmid & Kytömaa (1994), who showed that initial transient amplification of a disturbance does not imply instability in a Lyapunov sense (see Wang, Jackson & Sundaresan 1996 for further discussion). It is now clear that a uniform granular material in unbounded shearing motion is linearly unstable to layering modes, which lead to the formation of alternating layers of high and low particle concentrations oriented parallel to the plane of shear, provided the mean solids volume fraction is above a critical value.

Wang *et al.* (1996) considered a rapidly sheared layer of granular material confined between two parallel plates. They computed numerically the steady base-state solutions of the continuum equations of motion using the kinetic-theory-based constitutive model of Lun *et al.* (1984) and the boundary conditions proposed by Johnson & Jackson (1987) for various mean particle volume fractions, plate separations and material properties, and proceeded to investigate their stability characteristics. Depending on the nature of the particle–wall collisions and the operating conditions, a bounding wall may act either as a source or a sink of fluctuational, or pseudo-thermal, energy. These authors also considered an intermediate, although hypothetical, case where the particle–wall collisions were taken to be elastic and no slip was permitted between the particles and the bounding walls; in this situation, referred to as the case of adiabatic walls, the base-state corresponds to a uniform distribution of particles and constant shear rate. (We shall henceforth refer to this as the uniform solution.) Then the particles confined between the plates can be viewed as a slice of an infinite assembly of particles in plane shear. These authors computed numerically the base-state profiles for bounded shear flow and found that the state of uniform shear obtained for the case of adiabatic walls was only slightly altered when the walls were non-adiabatic. When the plate separation was sufficiently large, they reported that the deviation from uniform shear was confined to a small region near the walls. Furthermore, they found that the stability characteristics of the solutions obtained with non-adiabtic walls were very similar to those corresponding to the case of adiabatic walls. This suggested that the non-adiabaticity of the bounding walls (i.e. inelastic particle–wall collisions and slip at the wall) influences the results quantitatively, but not qualitatively.

More recently, Alam & Nott (1998) also studied the problem of plane Couette flow, and their findings differed from those of Wang *et al.* in some significant ways. They observed that, when the boundaries are non-adiabatic, solutions of the type reported by Wang *et al.* (1996) could be found only for modest plate separations. For large plate separations, their solutions exhibited a much larger degree of segregation than reported by Wang *et al.* (1996), and the stability characteristics of these solutions were markedly different from those of the corresponding adiabatic solutions. Thus, the bounding walls apparently had a both qualitative and quantitative influence on the stability characteristics. It now appears clear that base-state solutions of Wang *et al.* are incorrect for non-adiabatic boundaries, except for modest plate separations. However, their result that instabilities in the form of layering modes (alternating layers of high and low particle concentrations oriented parallel to the boundaries) are present regardless of the nature of the boundaries, provided the mean solids fraction is above a critical value of roughly 0.15, was verified to be correct by Alam & Nott (1998).

This tendency to form a segregated layer of density higher than the mean was indeed

observed in particle dynamics simulations by Tan (1995). Curiously, however, his simulations revealed that segregated layers evolve even when the mean particle volume fraction is small. This is in apparent conflict with the predictions of the continuum equations described above. Furthermore, Tan has reported instances where two layers of high solids fraction merge to form a single layer. Particle dynamics simulations of Hopkins & Louge (1991) and Tan & Goldhirsch (1997) reveal both axial and lateral structures. Particles tend to form aggregates (clusters), which interact with each other in a complex manner (Tan & Goldhirsch 1997). Under some conditions, one may also observe a churn-flow structure (Tan & Goldhirsch 1997).

The present study goes a step further in exploring the segregation patterns predicted by the continuum equations of motion for rapid granular flows. Specifically, we present a bifurcation analysis of the continuum equations to trace the family of steady fully developed solutions for plane Couette flow. In order to explore in detail the effects of wall properties on the solution structure, we treat the extent of non-adiabaticity as a parameter and determine the influence of this parameter on the bifurcation structure. Our analysis reveals clearly the structure of non-uniform, layered solutions permitted by adiabatic walls and explains how the (non-adiabatic) nature of the boundaries distorts the solution structure.

We also show that solutions with layered structures are possible for the case of adiabatic walls at low mean particle volume fractions, even though there are no bifurcations from the uniform solution at a finite Couette gap. These non-uniform solutions may be reached via finite-amplitude perturbations about the uniform solution, and we demonstrate this evolution by solving the full transient equations of motion. Thus we are able to explain the evolution of segregated layers at low mean densities as observed in the simulations of Tan (1995). Our transient solutions of the continuum equations also predict the merging of segregated layers that Tan has reported.

2. Governing equations

As in our earlier studies (Wang *et al.* 1996; Alam & Nott 1998), we will examine the stability of rapid plane shear of a granular material using the equations proposed by Lun *et al.* (1984). In the absence of gravity these equations take the following form:

$$\frac{\partial \rho}{\partial t} + \nabla \cdot (\rho \boldsymbol{u}) = 0,$$

$$\rho \frac{\mathrm{D}\boldsymbol{u}}{\mathrm{D}t} = -\nabla \cdot \boldsymbol{\sigma},$$

$$\tfrac{3}{2}\rho \frac{\mathrm{D}T}{\mathrm{D}t} = -\nabla \cdot \boldsymbol{q} - \boldsymbol{\sigma} : \nabla \boldsymbol{u} - J,$$

representing the balance of mass, momentum, and pseudo-thermal energy, respectively. Here ρ is the bulk density of the material, given by $\rho = \rho_p \nu$, where ν is the volume fraction of solids and ρ_p the density of the solid material; $\boldsymbol{u}$ is the mean velocity; $\boldsymbol{\sigma}$ is the stress tensor, defined in the compressive sense; T is the grain temperature, defined as $\frac{1}{3}\overline{u'^2}$, where u' is the fluctuation about the mean velocity; $\boldsymbol{q}$ is the flux of the pseudo-thermal energy and J represents the rate of dissipation of this energy, per unit volume, as a result of inelastic collisions between the particles. $\mathrm{D}/\mathrm{D}t$ denotes the convective derivative.

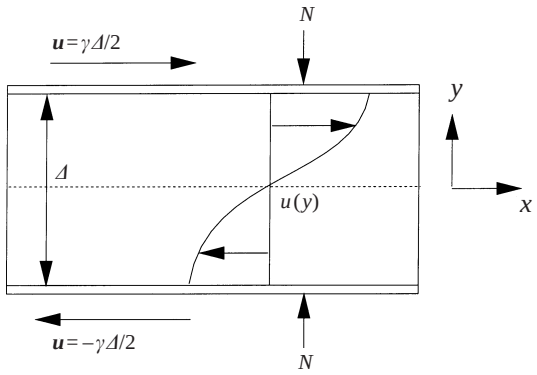

FIGURE 1. Schematic representation of shear flow of granular materials confined between two parallel plates.

Neglecting frictional contributions to the stress, we adopt the constitutive relations of Lun *et al.* (1984):

$$\boldsymbol{\sigma} = [\rho T(1 + 4\eta\nu g_0) - \eta\mu_b \nabla\cdot\boldsymbol{u}]\boldsymbol{I} - \left(\frac{2+\alpha}{3}\right)\left\{\frac{2\mu}{\eta(2-\eta)g_0}\left(1+\tfrac{8}{5}\nu\eta g_0\right)\left[1+\tfrac{8}{5}\eta(3\eta-2)\nu g_0\right]+\tfrac{6}{5}\eta\mu_b\right\}\boldsymbol{S},$$

$$\boldsymbol{q} = -\frac{\lambda}{g_0}\left\{\left(1+\tfrac{12}{5}\eta\nu g_0\right)\left[1+\tfrac{12}{5}\eta^2(4\eta-3)\nu g_0\right]+\frac{64}{25\pi}(41-33\eta)(\eta\nu g_0)^2\right\}\nabla T - \frac{\lambda}{g_0}\tfrac{12}{5}\eta(\eta-1)(2\eta-1)\left[1+\tfrac{12}{5}\eta\nu g_0\right]\frac{\mathrm{d}}{\mathrm{d}\nu}(\nu^2 g_0)\frac{T}{\nu}\nabla\nu,$$

$$J = \frac{48}{\pi^{1/2}}\eta(1-\eta)\frac{\rho_p \nu^2}{d} g_0 T^{3/2},$$

where $\boldsymbol{S}$ is the deviatoric part of the rate of deformation:

$$\boldsymbol{S} = \tfrac{1}{2}(\nabla\boldsymbol{u} + \nabla\boldsymbol{u}^T) - \tfrac{1}{3}\nabla\cdot\boldsymbol{u}\boldsymbol{I},$$

η is related to the coefficient of restitution, e_p, for particle–particle collisions by $\eta = (1 + e_p)/2$, while the two viscosity factors μ and μ_b, and the thermal conductivity factor λ, are given by

$$\mu = \frac{5M(T/\pi)^{1/2}}{16d^2}, \quad \mu_b = \frac{256\mu\nu^2 g_0}{5\pi}, \quad \lambda = \frac{75M(T/\pi)^{1/2}}{8\eta(41-33\eta)d^2},$$

where M and d are the mass and diameter of a particle respectively. Here, g_0 is the radial distribution function at contact, for which we choose the form used by Wang *et al.* (1996), namely

$$g_0(\nu) = \frac{1}{1-(\nu/\nu_m)^{1/3}},$$

where ν_m denotes the solids volume fraction at random close packing, taken to be 0.65. The value of the parameter α is set to 1.6, as in the work of Wang *et al.* (1996).

Figure 1 is a schematic of the problem under consideration, namely plane shear between two infinite parallel plates, and illustrates the choice of the coordinate system.

The relative velocity between the two plates is u_l, and the plates are separated by a distance Δ, so the apparent shear rate, γ, is equal to u_l/Δ. N denotes the normal force per unit area applied to each plate to maintain the plate separation constant at Δ. We now introduce dimensionless variables as follows:

$$(u^*, v^*) = \frac{(u, v)}{\gamma \Delta}, \quad \theta = \frac{T}{(\gamma d)^2}, \quad (X, Y) = (x, y)/\Delta, \quad \tau = \gamma t,$$

and this introduces one dimensionless group, $C = d/\Delta$, in the equations. Here u and v are the axial and transverse components, respectively, of the velocity vector $\boldsymbol{u}$. The scaling used here is the same as in Alam & Nott (1998).

In dimensionless form the equations of motion can be written as follows:

$$\frac{\partial \nu}{\partial \tau} + \frac{\partial (\nu u^*)}{\partial X} + \frac{\partial (\nu v^*)}{\partial Y} = 0,$$

$$\begin{aligned}
&\nu \left[\frac{\partial u^*}{\partial \tau} + u^* \frac{\partial u^*}{\partial X} + v^* \frac{\partial u^*}{\partial X} \right] \\
&\quad = -C^2 \frac{\partial (f_1 \theta)}{\partial X} + \frac{\partial}{\partial Y} \left[C^2 f_2 \theta^{1/2} \left(\frac{\partial u^*}{\partial Y} + \frac{\partial v^*}{\partial X} \right) \right] + \frac{\partial}{\partial X} \left[2C^2 f_2 \theta^{1/2} \left(\frac{2}{3} \frac{\partial u^*}{\partial X} - \frac{1}{3} \frac{\partial v^*}{\partial Y} \right) \right] \\
&\qquad + \frac{\partial}{\partial X} \left[C^2 \frac{8\nu^2}{3\pi^{1/2}} \eta g_0 \theta^{1/2} \left(\frac{\partial u^*}{\partial X} + \frac{\partial v^*}{\partial Y} \right) \right],
\end{aligned}$$

$$\begin{aligned}
&\nu \left[\frac{\partial v^*}{\partial \tau} + u^* \frac{\partial v^*}{\partial X} + v^* \frac{\partial v^*}{\partial Y} \right] \\
&\quad = -C^2 \frac{\partial (f_1 \theta)}{\partial Y} + \frac{\partial}{\partial X} \left[C^2 f_2 \theta^{1/2} \left(\frac{\partial u^*}{\partial Y} + \frac{\partial v^*}{\partial X} \right) \right] + \frac{\partial}{\partial Y} \left[2C^2 f_2 \theta^{1/2} \left(\frac{2}{3} \frac{\partial v^*}{\partial Y} - \frac{1}{3} \frac{\partial u^*}{\partial X} \right) \right] \\
&\qquad + \frac{\partial}{\partial Y} \left[C^2 \frac{8\nu^2}{3\pi^{1/2}} \eta g_0 \theta^{1/2} \left(\frac{\partial u^*}{\partial X} + \frac{\partial v^*}{\partial Y} \right) \right],
\end{aligned}$$

$$\begin{aligned}
&\tfrac{3}{2} \nu C \left[\frac{\partial \theta}{\partial \tau} + u^* \frac{\partial \theta}{\partial X} + v^* \frac{\partial \theta}{\partial Y} \right] \\
&\quad = \frac{\partial}{\partial X} \left[C^3 f_3 \theta^{1/2} \frac{\partial \theta}{\partial X} + C^3 f_4 \theta^{3/2} \frac{\partial v}{\partial X} \right] + \frac{\partial}{\partial Y} \left[C^3 f_3 \theta^{1/2} \frac{\partial \theta}{\partial Y} + C^3 f_4 \theta^{3/2} \frac{\partial v}{\partial Y} \right] \\
&\qquad - C f_5 \theta^{3/2} + C f_1 \theta \left(\frac{\partial u^*}{\partial X} + \frac{\partial v^*}{\partial Y} \right) + C f_2 \theta^{1/2} \\
&\qquad \times \left[\left(\frac{\partial u^*}{\partial Y} + \frac{\partial v^*}{\partial X} \right)^2 + \frac{4}{3} \left(\left(\frac{\partial u^*}{\partial X} \right)^2 - \left(\frac{\partial u^*}{\partial X} \right) \left(\frac{\partial v^*}{\partial Y} \right) + \left(\frac{\partial v^*}{\partial Y} \right)^2 \right) \right] \\
&\qquad + C \frac{8\nu^2}{3\pi^{1/2}} \eta g_0 \theta^{1/2} \left(\frac{\partial u^*}{\partial X} + \frac{\partial v^*}{\partial Y} \right)^2.
\end{aligned}$$

The first of these is the continuity equation, the next two are the two components of the momentum equation, and the last equation represents the pseudo-thermal energy balance. The functions f_1–f_8 are dimensionless and they depend only on ν, see table 1.

The boundary conditions for granular flows must reflect the fact that granular materials inevitably slip at the walls. Collisions of the particles with the walls dissipate

$$f_1(\nu) = \nu[1 + 4\eta\nu g_0(\nu)]$$

$$f_2(\nu) = \frac{(2+\alpha)5\pi^{1/2}}{288\eta(2-\eta)}\left(\frac{1}{g_0} + \frac{8}{5}\eta\nu\right)\left[1 + \frac{8}{5}\eta(3\eta-2)\nu g_0(\nu)\right] + \frac{8\eta\nu^2 g_0(\nu)(2+\alpha)}{15\pi^{1/2}}$$

$$f_3(\nu) = \frac{25\pi^{1/2}}{16\eta(41-33\eta)}\left\{\left(\frac{1}{g_0} + \frac{12}{5}\eta\nu\right)\left[1 + \frac{12}{5}\eta^2(4\eta-3)\nu g_0(\nu)\right] + \frac{64\eta}{25\pi}(41-33\eta)\eta^2\nu^2 g_0(\nu)\right\}$$

$$f_4(\nu) = \frac{25\pi^{1/2}}{16\eta(41-33\eta)}\left(\frac{1}{\nu g_0} + \frac{12}{5}\eta\right)\frac{12}{5}\eta(2\eta-1)(\eta-1)\frac{\mathrm{d}}{\mathrm{d}\nu}\left[\nu^2 g_0(\nu)\right]$$

$$f_5(\nu) = \frac{48\eta(1-\eta)\nu^2 g_0(\nu)}{\pi^{1/2}}, \quad f_6(\nu) = \frac{\pi\sqrt{3}\nu g_0(\nu)}{4\nu_m f_3(\nu)}$$

$$f_7(\nu) = \frac{\pi\nu g_0(\nu)}{2\sqrt{3}\nu_m f_3(\nu)}, \quad f_8(\nu) = \frac{\pi\nu g_0(\nu)}{2\sqrt{3}\nu_m f_2(\nu)}$$

TABLE 1. Dimensionless functions.

pseudo-thermal energy while slip at the walls generates pseudo-thermal energy. The balance of these determines the effect of the wall, which can be a source or a sink of pseudo-thermal energy.

Several studies have focused on the boundary conditions for granular flows (Hui *et al.* 1984; Johnson & Jackson 1987; Jenkins & Richman 1986; Richman 1988; Louge 1994; and Jenkins & Louge 1997). In the first two of these, the boundary conditions depend on only two wall properties: the coefficient of restitution for particle–wall collision e_w and a specularity coefficient ϕ'. In the other four papers the wall geometry is characterized in a detailed manner and the specularity coefficient is related to the details of the wall structure. However, the various models for the boundary interactions yield the same qualitative behaviour. In order to retain consistency with our earlier studies we use the boundary conditions of Johnson & Jackson (1987), which, in the absence of friction, assume the form

$$\boldsymbol{n}\cdot\boldsymbol{\sigma}\cdot\boldsymbol{t} + \left(\frac{\pi\sqrt{3}}{6\nu_m}\right)\phi'\rho_p\nu g_0 T^{1/2}u_{sl} = 0,$$

$$\boldsymbol{n}\cdot\boldsymbol{q} = \left(\frac{\pi\sqrt{3}}{6\nu_m}\right)\phi'\rho_p\nu g_0 T^{1/2}u_{sl} - \left(\frac{\pi\sqrt{3}}{4\nu_m}\right)(1-e_w^2)\rho_p\nu g_0 T^{3/2}.$$

The first boundary condition is obtained by equating the component of traction on the wall, in the direction of slip, to the rate of transfer of momentum to the wall by particle–wall collisions. The second boundary condition is found by equating the flux of pseudo-thermal energy from the wall to the difference between the rate of generation by slip and the rate of dissipation due to the inelasticity of the particle–wall collisions. Here $\boldsymbol{n}$ is the unit normal to the wall, pointing into the granular material, $u_{sl} = |\boldsymbol{u} - \boldsymbol{u}_w|$ where $\boldsymbol{u}_w$ is the velocity of the wall and $\boldsymbol{u}$ that of the granular material in contact with it, and $\boldsymbol{t}$ is a unit vector tangent to the wall, in the direction of the slip velocity. ϕ' is a 'specularity factor', which measures the fraction of the momentum of an incident particle in the direction of slip which is transmitted, on average, to the wall in a collision. e_w represents the coefficient of restitution for particle–wall collisions. The value of ϕ' is taken to be 0.6, as in the work of Wang *et al.* (1996).

The equations can be cast in a dimensionless form to obtain

$$u^* = \pm\left[\frac{C}{\phi' f_8}\frac{\mathrm{d}u^*}{\mathrm{d}Y} - 0.5\right] \text{ at } Y = \mp 0.5,$$

$$C^3\left(\frac{\mathrm{d}\theta}{\mathrm{d}Y} + \theta\frac{f_4}{f_3}\frac{\mathrm{d}v}{\mathrm{d}Y}\right) = \pm\left[C^2(1-e_w^2)f_6\theta - \phi' f_7(u^*+0.5)^2\right] \text{ at } Y = \mp 0.5.$$

It is convenient for the purpose of the present study to rewrite these boundary conditions in the following form:

$$u^* = \pm\left[\epsilon\frac{C}{\phi' f_8}\frac{\mathrm{d}u^*}{\mathrm{d}Y} - 0.5\right] \text{ at } Y = \mp 0.5, \tag{1}$$

$$C^3\left(\frac{\mathrm{d}\theta}{\mathrm{d}Y} + \theta\frac{f_4}{f_3}\frac{\mathrm{d}v}{\mathrm{d}Y}\right) = \pm\epsilon\left[C^2(1-e_w^2)f_6\theta - \phi' f_7(u^*+0.5)^2\right] \text{ at } Y = \mp 0.5, \tag{2}$$

where ϵ is an arbitrary parameter. Clearly, when ϵ is unity, we recover the Johnson & Jackson boundary conditions. When ϵ is set to zero, the particles are not allowed to slip at the wall and the net flux of pseudo-thermal energy from the wall to the particles becomes zero. The latter, hypothetical situation, is referred to as the *adiabatic* case (Wang *et al.* 1996; Alam & Nott 1998). The parameter ϵ is a continuation parameter that allows us to track the manner in which the solution structure varies as we go from the hypothetical adiabatic case ($\epsilon = 0$) to the Johnson & Jackson boundary conditions ($\epsilon = 1$). The solutions for intermediate values of ϵ do not correspond to any specific physical cases. Nevertheless, tracking the evolution of solutions as a function of ϵ exposes the underlying structure in a more clear fashion. As the walls are impervious to the particles, $\boldsymbol{u}\cdot\boldsymbol{n} = \boldsymbol{u}_w\cdot\boldsymbol{n}$. For our problem, it then follows that v^* is zero at both boundaries.

The adiabatic case has a simple steady-state solution (henceforth referred to as the base state) that exists for all values of C, namely

$$v = \text{constant} = \bar{v}, \quad u^* = Y, \quad v^* = 0, \quad \theta = f_2(\bar{v})/f_5(\bar{v}). \tag{3}$$

As mentioned earlier, this solution may be unstable under some conditions, giving rise to the evolution of non-uniform solutions. In general, the non-uniform structures can have axial and/or lateral structure. We have specifically excluded the modes having both lateral and axial structure or only axial structure by demanding that the disturbances be independent of X, the axial position. Thus, in the present study we are concerned only with the so-called layered solutions in which $v = v(Y,t)$, etc. Therefore, all the X-derivatives can be set to zero in the above system of equations.

When $\epsilon \neq 0$, even the base-state solution will become non-uniform: $v = v(Y)$, etc. Here also, we will concentrate on the fate of perturbations that depend only on Y: so, once again, the X-derivatives can be set to zero.

With this simplification, the equations of motion become

$$\frac{\partial v}{\partial \tau} + \frac{\partial (v v^*)}{\partial Y} = 0, \tag{4}$$

$$v\left(\frac{\partial u^*}{\partial \tau} + v^*\frac{\partial u^*}{\partial Y}\right) = \frac{\partial}{\partial Y}\left(C^2 f_2 \theta^{1/2}\frac{\partial u^*}{\partial Y}\right), \tag{5}$$

$$v\left(\frac{\partial v^*}{\partial \tau} + v^*\frac{\partial v^*}{\partial Y}\right) = \frac{\partial}{\partial Y}\left[C^2\left\{-f_1\theta + \frac{\partial v^*}{\partial Y}\left(\tfrac{4}{3}f_2\theta^{1/2} + \frac{8v^2}{3\pi^{1/2}}\eta g_0\theta^{1/2}\right)\right\}\right], \tag{6}$$

$$\tfrac{3}{2}\nu C\left(\frac{\partial\theta}{\partial\tau}+v^*\frac{\partial\theta}{\partial Y}\right)=\frac{\partial}{\partial Y}\left[C^3f_3\theta^{1/2}\frac{\partial\theta}{\partial Y}+C^3f_4\theta^{3/2}\frac{\partial v}{\partial Y}\right]-Cf_5\theta^{3/2}$$
$$+C\left\{-f_1\theta\frac{\partial v^*}{\partial Y}+f_2\theta^{1/2}\left[\left(\frac{\partial u^*}{\partial Y}\right)^2+\frac{4}{3}\left(\frac{\partial v^*}{\partial Y}\right)^2\right]\right.$$
$$\left.+\frac{8\nu^2}{3\pi^{1/2}}\eta g_0\theta^{1/2}\left(\frac{\partial v^*}{\partial Y}\right)^2\right\}. \tag{7}$$

3. Numerical scheme

We have used several computational schemes, in order to verify the accuracy of our calculations and ascertain that the computed results are not artifacts of any specific numerical discretization procedure. Three of the methods we have used are: a second-order finite difference method, a Galerkin finite element method, and a Chebyshev–Tau Galerkin method. We will not present the details of the finite difference scheme as it is relatively straightforward.

The Chebyshev–Tau Galerkin approximation requires the expansion of a dependent variable β in the following manner:

$$\beta(\xi,t)=\sum_{k=0}^{N}a_k(t)T_k(\xi).$$

We substitute the expansions into the equation of motion and form the inner product of the resulting equations with each of the $N+1$ Chebyshev polynomials. The integrals are evaluated using the inverse discrete Chebyshev transform, which uses the Gauss–Lobatto collocation points for all equations of motion.

The imposition of the boundary conditions and the mean volume fraction generates a set of algebraic constraints which supplement the differential equations for the coefficients $a_k(t)$. Further details on the implementation of this scheme can be found in Canuto *et al.* (1988)

The Galerkin finite element method is essentially similar, with the main difference being that the expansion of the variables is in terms of *local* basis functions (see, for example, Reddy 1984). We employed Hermite cubic basis functions and used Gaussian quadrature for the integration.

4. Results

4.1. *Bifurcation analysis: adiabatic boundaries*

The dimensionless base-state solution described by (3) depends only on $\bar{\nu}$ and e_p. Its stability is influenced by an additional parameter, namely the dimensionless plate separation $1/C$, see (4)–(7). Alam & Nott (1998) showed that the eigenfunctions for the linearized equations are

$$\left.\begin{aligned}\hat{\nu}(y)&=\hat{\nu}_1\cos k_n(y\pm\tfrac{1}{2}), &\quad \hat{\theta}(y)&=\hat{\theta}_1\cos k_n(y\pm\tfrac{1}{2}),\\ \hat{u}(y)&=\hat{u}_1\sin k_n(y\pm\tfrac{1}{2}), &\quad \hat{v}(y)&=\hat{v}_1\sin k_n(y\pm\tfrac{1}{2}),\end{aligned}\right\} \tag{8}$$

where $k_n=n\pi$, and the mode number n is a positive integer. The even modes correspond to eigenfunctions of v and θ that are symmetric about the mid-plane (those of u^* and v^* are antisymmetric) and the odd modes correspond to eigenfunctions of v and θ that are anti-symmetric (those of u^* and v^* are symmetric). Substitution of

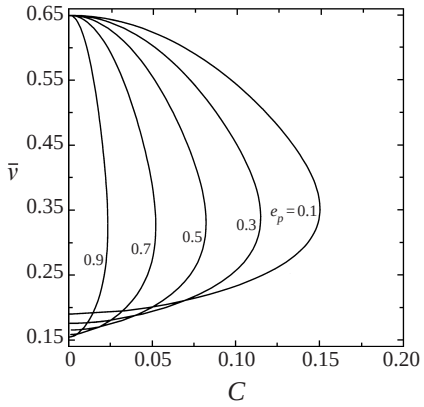

FIGURE 2. Marginal stability contours for different values of e_p. Adiabatic walls. In each case, the uniform base state is linearly stable in the region to the right of the marginal stability contour.

the above in the linearized governing equations gives a dispersion relation that is quartic in the eigenvalue ω, and the least-stable eigenvalue for all n is purely real. The condition of marginal stability for mode n then is (equation (5.10) in Alam & Nott 1998),

$$\left(\frac{1}{C}\right)^2 = \frac{N_1}{N_2} k_n^2, \tag{9}$$

where

$$N_1 = \frac{1}{f_5}\left(f_3 - \frac{f_1}{f_1'} f_4\right) \quad \text{and} \quad N_2 = \left(\frac{f_5'}{f_5} + \frac{f_2'}{f_2}\right)\frac{f_1}{f_1'} - 2,$$

with the functions f_1–f_5 evaluated at $\nu = \bar{\nu}$ and the primes indicating derivatives with respect to ν. For fixed values of the mean density $\bar{\nu}$ and e_p, it is then clear from (9) that as the plate separation $1/C$ is increased, the $n = 1$ mode will be the first to become unstable at $C_c = 2\pi(N_2/N_1)^{1/2}$, and successive modes become unstable after intervals of C_c. Hence there will be simple bifurcations from the uniform solution at intervals of C_c in the plate separation in a bifurcation diagram showing steady-state solutions, and the bifurcating branches will represent alternately asymmetric and symmetric solutions (see, for example, figure 14).

For the sake of clarity in exposition of our results, in what follows we shall concentrate mainly on symmetric perturbations (i.e. even values of n) and the steady-state solutions that arise from them, and address asymmetric solutions in § 4.4. The locus of marginal stability for symmetric perturbations in the $(\bar{\nu}, C)$-plane is due to the $n = 2$ mode, which is shown in figure 2 for different values of e_p. For specified $\bar{\nu}$ and e_p, the base state is linearly stable for large C (small plate separations) and as C is decreased it becomes unstable. Note that the region of instability of the uniform solution expands as the coefficient of restitution is decreased. This trend can be attributed to the fact that the instability is caused by the inelastic nature of the particle–particle collisions. Figure 2 also illustrates the result that there are no layering instabilities below a mean solids fraction of roughly 0.156, regardless of the value of e_p.

The above result indicating the stability of the uniform solution for low $\bar{\nu}$ is not borne out by the simulations of Tan (1995); figure 3 shows the evolution of a non-uniform structure in his simulation of shear flow for a mean particle volume fraction

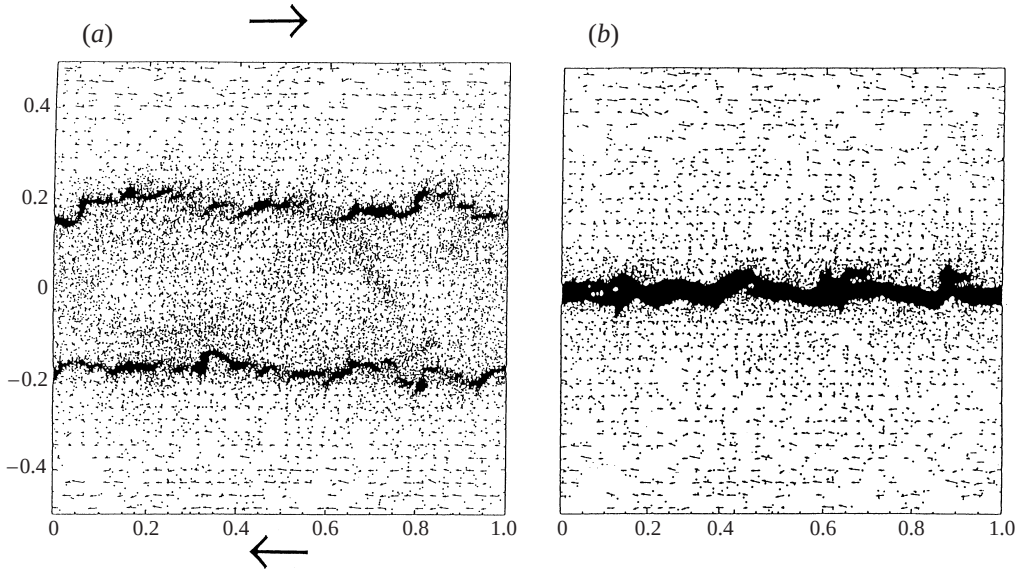

FIGURE 3. Particle dynamics simulation of shear flow of inelastic disks by Tan (1995). Panel (*a*) reveals the formation of two dense layers of disks, which subsequently coalesce to give a single layer shown in panel (*b*). $\overline{v} = 0.05$; $e_p = 0.6$; $C = 0.00089$.

of 0.05. His simulations were started with a nearly uniform assembly of disks confined between two stationary parallel plates and assigned an initial velocity distribution with zero mean. The apparent shear rate was then increased from zero to a desired final value in an exponential manner and the evolution of the structure was followed by particle dynamics simulations. It was found that two dense plugs formed in the vicinity of the walls and slowly travelled towards the centreline (figure 3*a*), eventually merging into a single dense plug (figure 3*b*). This central plug persisted even if the apparent shear rate was lowered. This suggests the possibility of stable non-uniform structures, even in dilute systems. The linear stability analysis, summarized in figure 2, indicates that the base state is linearly stable for $\overline{v}$ less than roughly 0.15. This then raises doubts about the validity of the continuum equations based on the kinetic theory of granular materials, as they appear to predict a qualitatively incorrect behaviour.

In an attempt to compute the steady-state solutions that the layering instabilities lead to and to also look into the possibility of segregation at low $\overline{v}$, we carried out a bifurcation analysis of the equations of motion and computed, by numerical continuation techniques (Doedel, Keller & Kernevez 1991), families of fully developed non-uniform solutions. As described below, the continuum equations do indeed predict the existence of layered solutions even at low values of $\overline{v}$. In this section, we will consider only solutions in which v and θ are symmetric about $Y = 0$.

The bifurcation diagram for $e_p = 0.8$ and $\overline{v} = 0.35$ is presented in figure 4. This shows the particle volume fraction at the centreline, $v(Y = 0)$ as a function of the bifurcation parameter C. As the walls are adiabatic, the uniform solution given by $v = 0.35$ is possible for all C (see equation (3)) and this branch is shown by the horizontal line $v(Y = 0) = 0.35$. This state is linearly stable for large C, and as one decreases C it loses stability through a *supercritical pitchfork bifurcation*; a real eigenvalue crosses the imaginary axis from the left half-plane into the right half-plane.

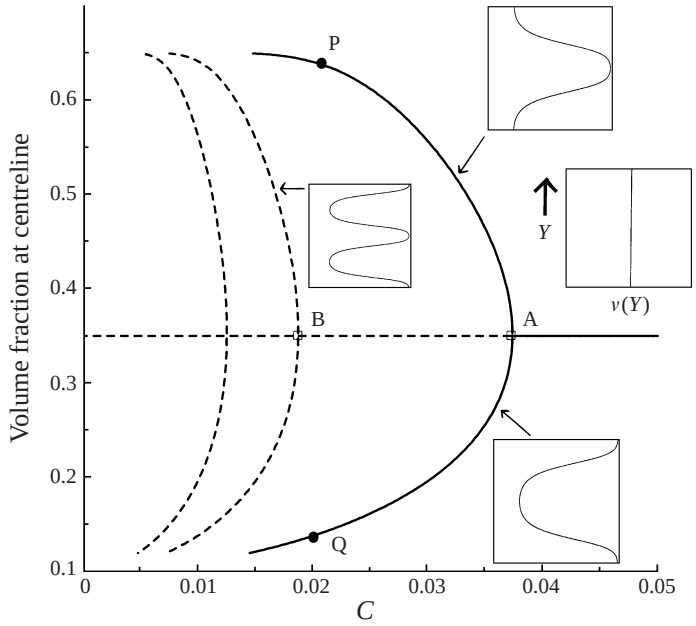

FIGURE 4. Bifurcation diagram for $e_p = 0.8$, $\bar{\nu} = 0.35$ and adiabatic walls: ——, stable; - - -, unstable.

The branches that originate from this bifurcation point represent stationary solutions corresponding to the even modes in (9). In this figure, the uniform solution to the right of point A is shown by a solid line to indicate linear stability, while it is shown by a dashed line to the left of A to indicate that it is now linearly unstable.

Two stable solution branches originate at the bifurcation point (A). These branches correspond to fully developed layered solutions, i.e. solutions with structure only in the Y-direction. The upper branch corresponds to a solution with a dense region at the centre and a dilute region near the walls. The lower branch corresponds to a solution which has a dense region of particles near the wall and a dilute region at the centre. As the plate separation is increased the solutions show a greater degree of segregation. The $\nu(Y)$ profile of the solutions is shown schematically in the insets.

Other bifurcations, corresponding to the points of marginal stability of the $n = 4, 6$ and higher even modes, arise at lower values of C. Thus, for example, two layered solutions bifurcate out of the uniform state at point B where the value of C is half of that at point A. The density profiles for these solutions have two 'humps' between the restraining plates, and each of these humps corresponds exactly with a single-hump layered solution at twice the value of C (emerging from point A). In other words, the solution at any point in the branches originating from point B is a periodic replication of the solution at half the value of C in the branches originating from point A. Similarly a three-humped solution emerges at one-third of the value of C at point A and so on. The first two pairs of branches of multiple-humped solutions are shown in figure 4. Note that these solutions, shown by broken lines, are unstable to disturbances with a single hump. Therefore these branches are of less interest than those emerging from point A; for this reason we will present results for only the first pair of branches bifurcating from the uniform solution (i.e. the branches originating from point A in figure 4) in what follows.

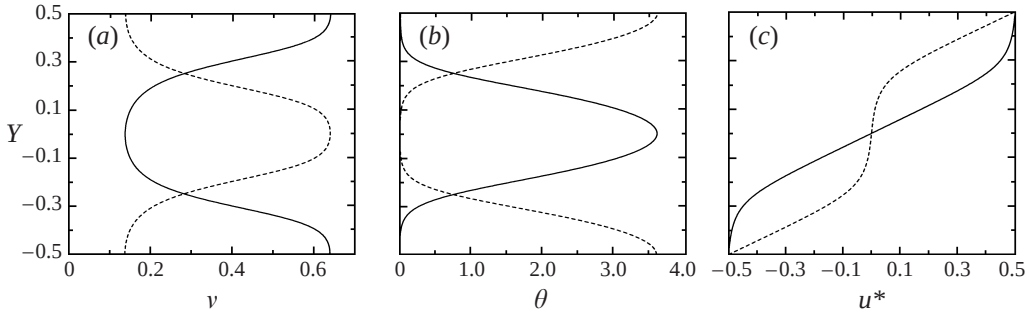

FIGURE 5. The structure of fully developed solutions corresponding to points P (broken lines) and Q (solid lines) in figure 4. $C = 0.02$. (*a*) Particle volume fraction, (*b*) pseudo-thermal temperature, (*c*) axial velocity.

Figure 5 shows the structures of the two fully developed solutions at $C = 0.02$ (points P and Q in figure 4). It is clear that the solution corresponding to point P lying in the upper primary branch in figure 4 consists of a dense plug of solids in the vicinity of $Y = 0$, while the solution at point Q in the lower branch of figure 4 has a pair of dense plugs near the walls (see figure 5*a*). The pseudo-thermal energy is low in regions of high v, and vice versa, and this is an immediate consequence of the Y-momentum balance. It is apparent from figure 5(*c*) that the velocity gradient is very small in the dense regions.

When the walls are adiabatic, they play no special role in influencing the solution structure. Indeed, one can view the granular material confined between the walls as a slice of an unbounded granular material under shear. To be specific, solutions of the adiabatic problem can be 'stacked' together to create a solution for the unbounded problem. The volume fraction and granular temperature profiles in such solutions will naturally be periodic in the Y-direction with a dimensionless wavelength of unity. The two solutions presented in figure 5 yield the same layered solution for unbounded flow, the only difference being that they are out of phase by half a wavelength. Thus the two branches bifurcating from point A in figure 4 differ only by this phase shift. The same is true for the branches emerging from point B and so on. The important point to note is that the adiabatic wall does not discriminate between the two branches separated by this phase shift. We shall see later that when the walls are non-adiabatic, the two solutions no longer differ by only a phase shift, and that one of the branches is chosen as the primary branch.

Figure 6 shows the bifurcation structure for various mean particle volume fractions in the limit of adiabatic walls. (As per our discussion earlier in connection with figure 4, only the primary branches which represent solutions with a single density maximum are shown.) For large $\overline{v}$ values, the bifurcation is supercritical (see panels *a–d*). However, as $\overline{v}$ is decreased, the bifurcation becomes *subcritical* (panels *e*, *f*), thus creating a region to the right of the bifurcation point in which three stable solutions and two unstable ones coexist.

Irrespective of whether the bifurcation is supercritical or subcritical, the magnitude of the non-uniformity in the layered solution branch is small in the vicinity of the bifurcation point, and it becomes progressively more pronounced as we move further along this branch.

It is instructive to examine how the bifurcation point, where the layered solutions emerge from the base state, moves as we change $\overline{v}$. It can be seen from figure 6 that the

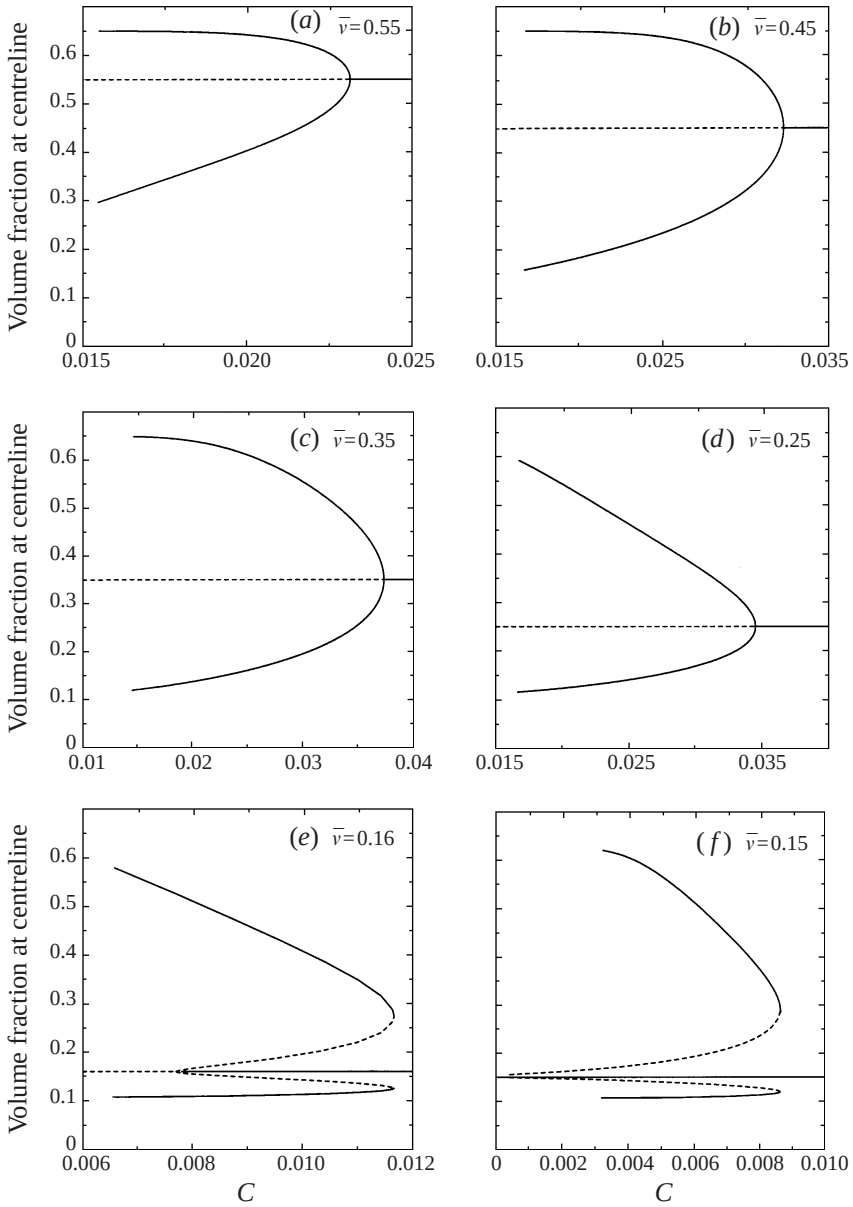

FIGURE 6. The bifurcation diagrams for various values of $\overline{\nu}$. $e_p = 0.8$. Adiabatic walls. Only the uniform solutions and the single-hump branches bifurcating from the uniform solution are shown.

value of C corresponding to this bifurcation point first increases as $\overline{\nu}$ is decreased from a large value, then reaches a maximum and subsequently recedes towards zero. This is to be expected from the marginal stability contours shown in figure 2. According to linear stability analysis, the bifurcation point reaches $C = 0$ when $\overline{\nu} = \overline{\nu}_* \approx 0.156$ for the case $e_p = 0.8$, shown in figure 6. Thus, figure 6(f) illustrates a situation where layered solutions coexist with a uniform state which is linearly stable for all $C > 0$.

It can be ascertained through a linear stability analysis of the base state that the real part of the leading eigenvalue tends to zero as $C \to 0$ for any $\overline{\nu}$. Therefore, the

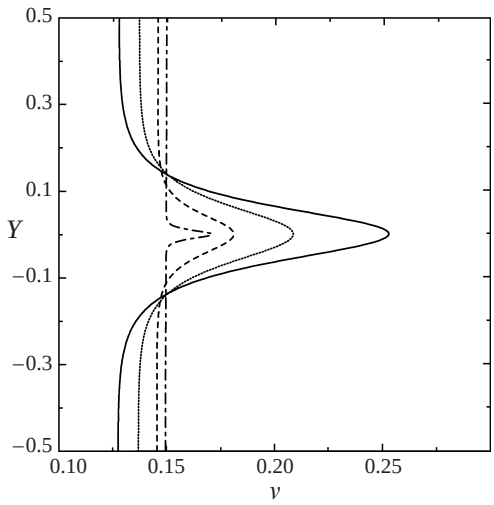

FIGURE 7. The variation of v as a function of Y for several different values of C. $\bar{\nu} = 0.15$, $e_p = 0.8$: ——, $C = 0.008$; – – –, $C = 0.006$; - - -, $C = 0.002$; – - –, $C = 0.00043$.

bifurcation obtained in the case of low $\bar{\nu}$ values, where the base state is linearly stable for all $C > 0$, belongs to the category of *bifurcations from infinity* (Rosenblat & Davis 1979, see the Appendix for further details). Accordingly, the bifurcation point remains pinned at the origin when $\bar{\nu} < \bar{\nu}_*$, and layered solutions bifurcate from $C = 0$ for all values of $\bar{\nu}$ in his range.

We conclude that layered, non-uniform solutions are indeed predicted at low values of $\bar{\nu}$ by a continuum description for rapid granular flow, even though the uniform base state is linearly stable. Needless to say, these solutions can arise only when the plate separation is sufficiently large or, equivalently, C is sufficiently small (see figure 6f). For such values of C, a sufficiently large disturbance to the (linearly stable) uniform state can drive the system to one of the layered solutions, as a result of the nonlinear terms in the equations. Therefore it should indeed be possible to capture behaviour of the type presented in figure 3, as our transient analysis below demonstrates.

Figure 7 shows the profile of v for points on the upper unstable branch in figure 6(f). As C approaches zero, the v-profile becomes flatter and flatter and the hump less and less pronounced. This suggests that, the smaller the value of C, the smaller is the amplitude of the disturbance which may be able to drive a dilute system away from the uniform state to the layered state.

We have performed calculations such as those shown in figure 6 for several other values of e_p. In general, as e_p is decreased, the range of values of C for which the system admits stable layered solutions becomes larger. This is consistent with the results of the linear stability analysis presented in figure 2.

4.2. *Transient simulations: adiabatic boundaries*

We now turn our attention to the evolution of non-uniform layered solutions, as predicted by equations (1), (2), (4)–(7). As in the bifurcation analysis of the previous subsection, we restrict attention to solutions which preserve the symmetry of v and θ about the centreline. The initial condition is obtained by perturbing the uniform state by adding a small multiple of the eigenfunction corresponding to the dominant eigenvalue of the uniform state, scaled so that the maximum value of Δv is 0.01. As

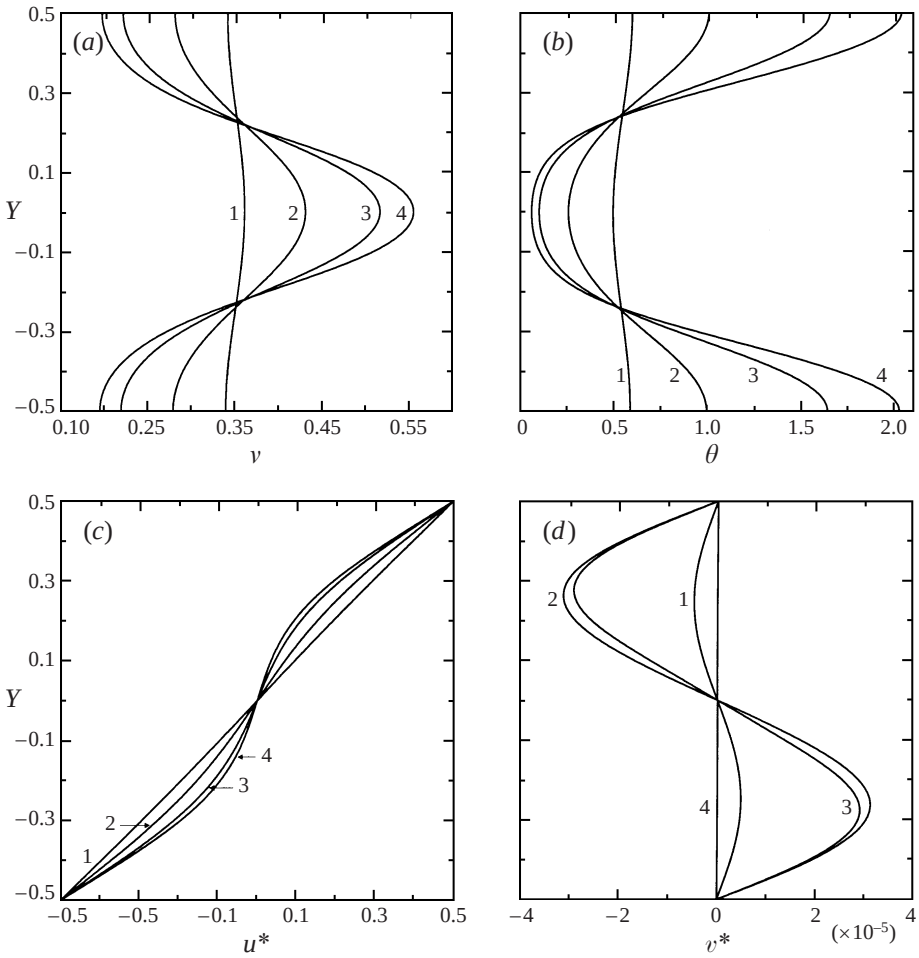

FIGURE 8. Evolution of layered solution from an unstable uniform state. $\overline{v} = 0.35$; $e_p = 0.8$; $C = 0.03$. Curve 1: $\tau = 0$; Curve 2: $\tau = 2000$; Curve 3: $\tau = 3000$; Curve 4: $\tau = 6000$.

the growth rate of this eigenmode is quite small the solution takes a long time (about 5000 dimensionless time units) to develop. The eigenfunction which has been added to the uniform solution represents an increase in the particle concentration in the centre and a depletion near the boundaries (curve 1, figure 8*a*), while the opposite is true for the granular temperature (curve 1, figure 8*b*). The perturbation to the axial velocity profile is very small (curve 1, figure 8*c*). The perturbation in the transverse velocity is such that it tends to convect the particles away from the boundaries and towards the centreline (curve 1, figure 8*d*). It is clear from figure 8 that the particle volume fraction increases gradually in the centre where the particles are also becoming less thermally active. Appreciable nonlinearity develops in the axial velocity profile; the region of high concentration shears much less than the dilute region.

If we reverse the sign of the initial perturbation in figure 8, so that the initial condition now consists of a depletion of particles in the centre and an increase in the concentration near the boundaries, the system will evolve to the other fully developed state in which a pair of dense plugs is located near the boundaries (see figure 5).

In the example considered in figure 8 ($\overline{v} = 0.35$, $e_p = 0.8$, $C = 0.03$), the uniform

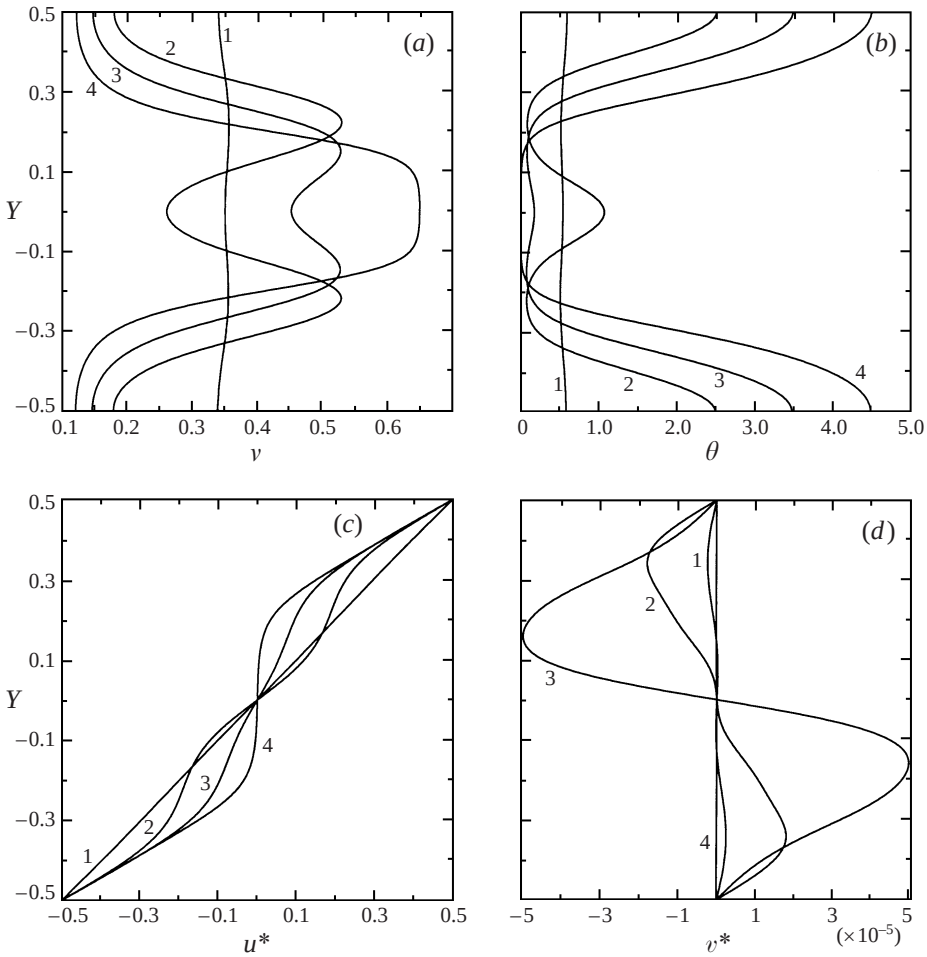

FIGURE 9. Transient evolution of layered solution from a uniform base state. $\bar{v} = 0.35$; $e_p = 0.8$; $C = 0.015$. Both the single-hump mode, and the dominant two-hump mode were excited initially. Curve 1: $\tau = 0$; Curve 2: $\tau = 4000$; Curve 3: $\tau = 6000$; Curve 4: $\tau = 10\,000$.

state was unstable and the dominant eigenmode involved only a single hump; when this mode was excited the system evolved smoothly to the layered structure shown there. If we consider the same uniform state ($\bar{v} = 0.35$, $e_p = 0.8$), but increase the plate separation by a factor of two (so that $C = 0.015$), the uniform state is still unstable; however, the dominant eigenmode now contains two humps in v located on either side of the centreline. When this mode is excited along with the eigenmode involving only a single hump (curves labelled 1 in figure 9*a–d*), the double-humped mode grows faster, producing two plugs (curves 2 in these plots). However, these plugs slowly coalesce to produce a single central plug, as the two-humped solution is linearly unstable. Thus the continuum equations do capture the formation of multiple plugs (during transients) which subsequently coalesce, as observed in the simulations of Tan (1995).

In the above examples, the base states are linearly unstable to a layering instability so any small disturbance will drive the system toward a layered solution. Let us now consider a different example with $\bar{v} = 0.15$, $e_p = 0.9$, $C = 0.005$, when a linearly stable

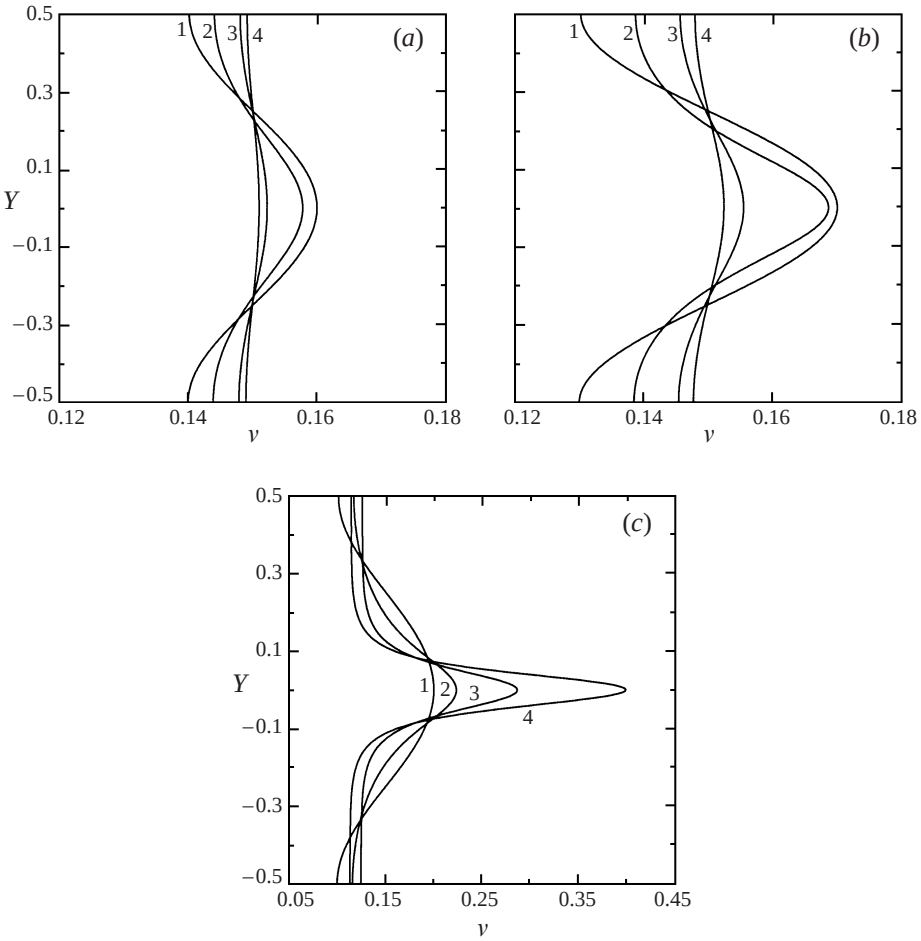

FIGURE 10. Transient evolution of volume fraction profile following different initial perturbations of the base (uniform) state. $\bar{v} = 0.15$; $e_p = 0.9$; $C = 0.005$. The initial perturbations are obtained by scaling the eigenfunction corresponding to the dominant eigenvalue so that the maximum variation in particle volume fraction (v) is (*a*) 0.01; (*b*) 0.02; (*c*) 0.05. Panels (a, b): Curve 1: $\tau = 0$; Curve 2: $\tau = 25\,000$; Curve 3: $\tau = 100\,000$; Curve 4: $\tau = 150\,000$. Panel (*c*): Curve 1: $\tau = 0$; Curve 2: $\tau = 5000$; Curve 3: $\tau = 25\,000$; Curve 4: $\tau = 150\,000$.

base state coexists with a stable fully developed layered solution (see figure 6). Then one can anticipate that very small perturbations of the base state will decay, while sufficiently large disturbances will grow and develop into the stable layered solution. This is illustrated in figures 10(*a–c*), where the temporal evolution of the system following three different initial perturbations is shown. As in the previous examples, the perturbations consist of small multiples of the eigenfunction corresponding to the dominant eigenvalue. For small initial perturbations, shown in panels (*a*) and (*b*), the perturbations decay, and the uniform state is recovered asymptotically. However, if the perturbation is sufficiently large, as in panel (*c*), the perturbations grow and the layered solution is obtained at large times.

While the above examples illustrate the manner in which layers can develop, the initial conditions considered in them differ from those investigated by Tan (1995). In spite of this difference, it is easy to recognize that results of the type observed by Tan

can be captured in a qualitatively correct manner by the continuum equations and this has been further verified by Agrawal (1999).

4.3. *Bifurcation analysis: non-adiabatic boundaries*

The adiabatic boundary conditions considered above are artificial; one expects the particle–wall collisions to be inelastic in general, and some slip to occur at the walls. As noted earlier, when ϵ in equations (1) and (2) is set to zero, the walls become adiabatic, while setting ϵ to unity recovers the boundary conditions of Johnson & Jackson (1987). In order to understand how the non-adiabatic nature of the particle–wall interactions affects the flow characteristics, we treat ϵ as a parameter and trace its influence on the bifurcation structure described in § 4.1.

Figure 11(*a*) shows the bifurcation structure for $\overline{v} = 0.35$, $e_p = 0.8$, $e_w = 1$ and $\epsilon = 0.1$. The walls in this case act as a weak source of pseudo-thermal energy. Three branches (1, 2 and 3) of solutions for this case are shown by the thick lines, while the thin lines show the bifurcation structure for adiabatic walls ($\epsilon = 0$). Clearly, the solution branches have detached themselves from one another when ϵ is made non-zero. As ϵ increases, they recede further away from the uniform solution branch of the adiabatic case. If we regard the bifurcation structure in the adiabatic case as being *perfect* (Strogatz 1994, p. 69) we see that it develops imperfections when the walls become non-adiabatic. The branches which are linearly stable to one-dimensional perturbations with centreline symmetry in v and θ are shown by solid lines, while those that are unstable to such perturbations are indicated by broken lines.

Figure 11(*b*) shows the bifurcation structure for $\epsilon = 1$. In this case the branches have receded quite far from the uniform solution branch of the adiabatic case. We see that there are no longer any solutions with small spatial variations in v, except when the plate separation is very small. In this figure, branch 1 corresponds to the layered solution with the plug in the middle; branch 2 is curled up so that the top portion is unstable while the bottom portion is stable. Branch 3 has also curled up, but in this case the entire branch is unstable.

We next consider the bifurcation structure when the boundaries act as sinks of pseudo-thermal energy. This bifurcation structure, shown in figure 12(*a*) for $\overline{v} = 0.35$, $e_p = 0.8$, $\epsilon = 0.01$ and $e_w = 0.5$, is essentially a distorted reflection of figure 11(*a*) about $v = 0.35$. Figure 12(*b*) shows the bifurcation structure for non-adiabatic boundary conditions with $\epsilon = 1$. A comparison of figures 11 and 12 clearly reveals how the nature of the walls selects the primary solution branch, defined here as that branch which exists for all values of C (i.e. branch 1 in figures 11 and 12). When the boundaries are adiabatic, the primary branch is simply the uniform solution and the layered solutions bifurcate from this branch. The imperfection introduced by the boundaries is such that when they act as sources of pseudo-thermal energy, the layered branch with a dense plug of grains in the middle becomes the primary branch; when the walls act as sinks of pseudo-thermal energy, the layered branch with high particle concentrations in the vicinity of the two walls is selected as the primary branch.

Particle volume fraction profiles along the primary solution branches of the cases of source and sink walls (that is, branch 1 in figures 11 and 12) at two different values of C are presented in figure 13. Figure 13(*a*) corresponds to a relatively small plate separation; for source (sink) walls the volume fraction near the wall is slightly lower (higher) than that in the adiabatic case, while the opposite is true in the centre region. The volume fraction profile in the primary branch with source walls, at $C = 0.014$, is shown in figure 13(*b*); also shown in this figure is the layered solution of the adiabatic

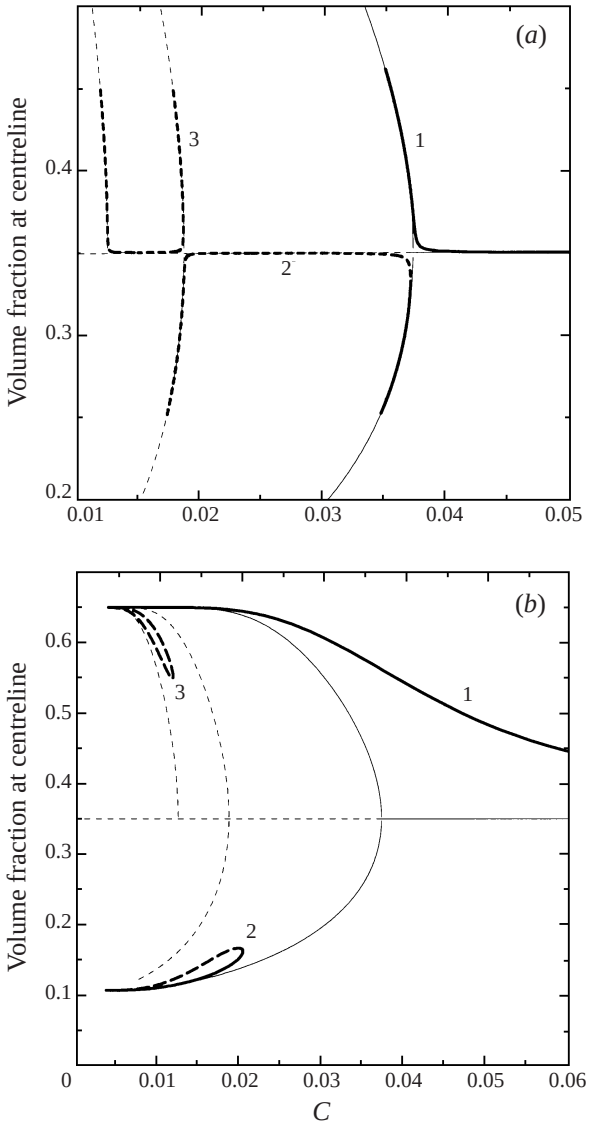

FIGURE 11. The effects of boundaries on the bifurcation structure. The boundaries act as sources of pseudo-thermal energy. $\bar{\nu} = 0.35$; $e_p = 0.8$; $e_w = 1.0$. (*a*) Results for $\epsilon = 0$ (thin lines) and $\epsilon = 0.1$ (thick lines). (*b*) Results for $\epsilon = 0$ (thin lines) and $\epsilon = 1.0$ (thick lines).

problem with a plug in the centre. The similarity between the two profiles is striking, making it abundantly clear that the principal role of the wall has been to *select the primary branch*. Figure 13(*c*) compares volume fraction profiles on the primary branch for the case of sink walls with the corresponding solution in the adiabatic case, with plugs at the boundaries. It reinforces this conclusion.

Wang *et al.* (1996) found that the base-state solutions obtained over a wide range of plate separations for the case of adiabatic boundaries were only slightly modified when the walls were made non-adiabatic (see figure 2 in their paper). This was disputed by Alam & Nott (1998), who suspected that this finding was likely to be a consequence of inadequate numerical accuracy. The present study, employing three

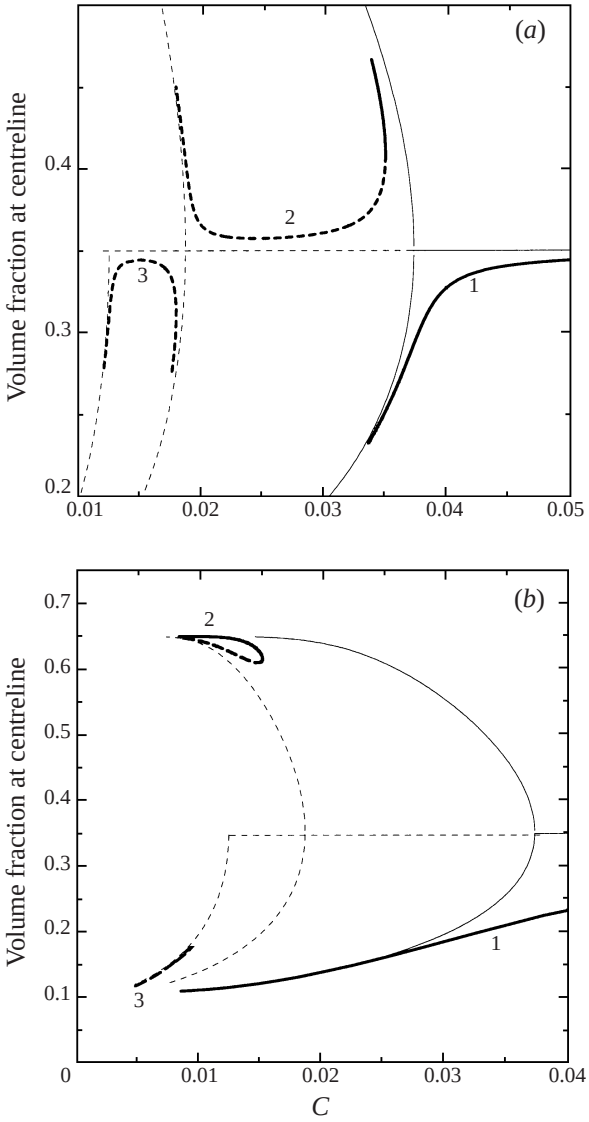

FIGURE 12. The effects of boundaries on the bifurcation structure. The boundaries act as sinks of pseudo-thermal energy. $\bar{\nu} = 0.35$; $e_p = 0.8$; $e_w = 0.5$. (*a*) Results for $\epsilon = 0$ (thin lines) and $\epsilon = 0.01$ (thick lines). (*b*) Results for $\epsilon = 0$ (thin lines) and $\epsilon = 1.0$ (thick lines).

different numerical schemes to rule out numerical artifacts, establishes clearly that the solutions of the type found by Wang *et al.* are possible only for small plate separations. The imperfect bifurcations brought about by the non-adiabatic nature of the bounding walls eliminate solutions of this type for large separations. Therefore, for the cases where the walls act as sources or sinks of pseudo-thermal energy, the stability studies of Wang *et al.* are erroneous, as they are based on perturbations about incorrect steady states. On the other hand, all the results of Wang *et al.* for adiabatic boundaries are correct, as has been verified by Alam & Nott (1998) and the present authors.

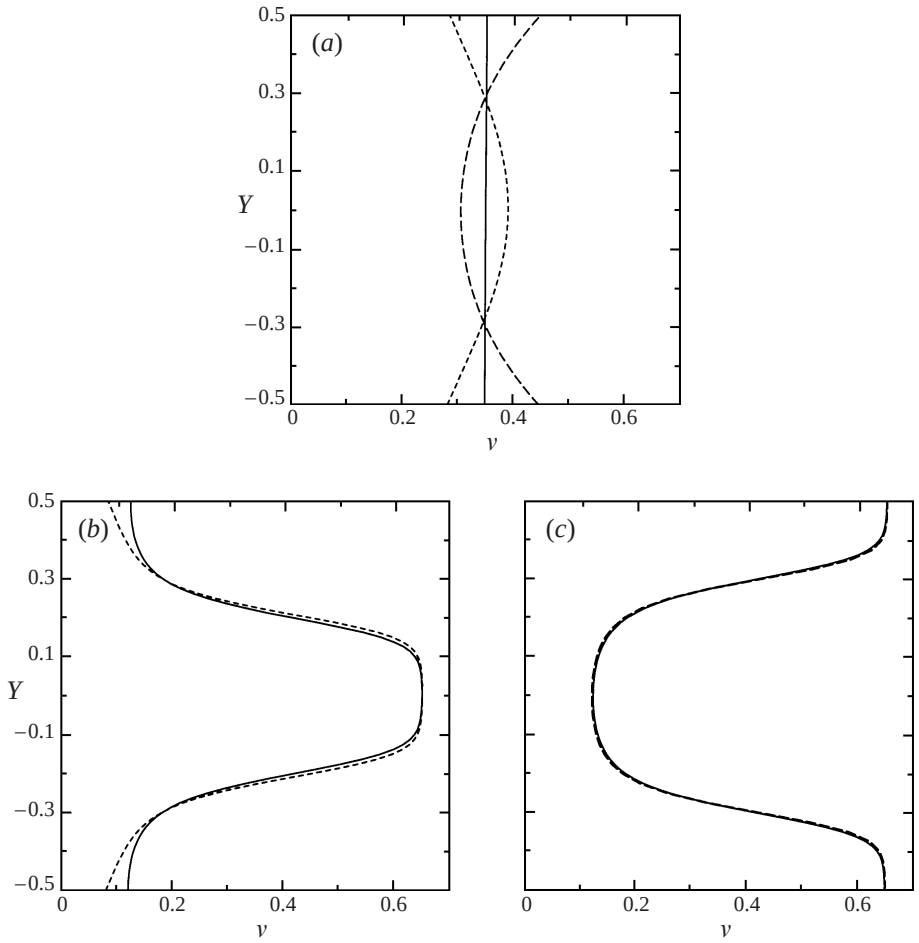

FIGURE 13. The effects of boundaries on the particle volume fraction profile. $\bar{\nu} = 0.35$; $e_p = 0.8$. (*a*) $C = 0.1$, (*b*, *c*) $C = 0.014$. ——, adiabatic; - - -, source walls, $e_w = 1.0$; – – –, sink walls, $e_w = 0.5$.

4.4. *Asymmetric layered solutions*

In the results presented thus far, we have restricted attention to solutions with ν symmetric about the centre-plane of the sheared layer. Dropping this requirement we find that, in addition to the symmetric solutions, there exist asymmetric layered solutions. These come in pairs which, due to the absence of gravity in our analysis, are physically identical, and are merely reflections of each other about the centre-plane.

The bifurcation diagram for $\bar{\nu} = 0.35$, $e_p = 0.8$ and adiabatic boundaries is shown in figure 14 where we have included both symmetric and asymmetric solutions (only the first few layered solution branches are shown). The insets show schematically the ν-profiles for some of the branches. The primary asymmetric branch, arising from the $n = 1$ instability of (9), emerges from the uniform state at $C = 0.074$, which is twice the value of C at which the primary symmetric branches bifurcate from the uniform solution. As mentioned earlier, there are two asymmetric branches bifurcating at $C = 0.074$, both having the same $\nu(Y = 0)$ since they are reflections of each other about the central plane, and they are therefore superimposed in the bifurcation diagram. The same is true for the secondary asymmetric branch (bifurcating at

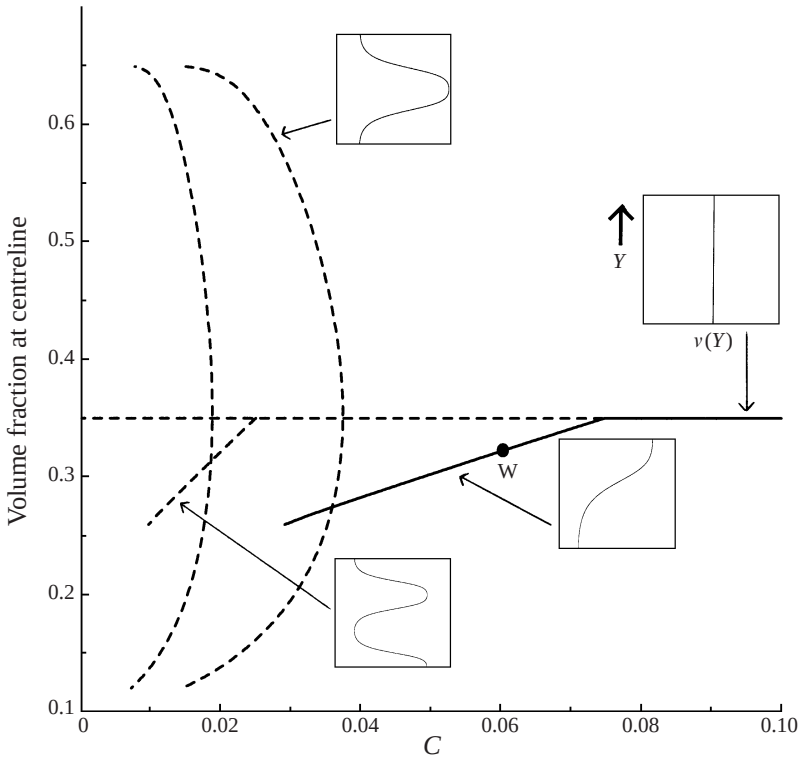

FIGURE 14. Bifurcation diagram showing both symmetric and asymmetric branches. The boundaries are assumed to be adiabatic. $\bar{\nu} = 0.35$; $e_p = 0.8$. The insets show the structures of the solutions for the indicated branches.

$C = 0.0247$), and so on. The stability characteristics of the various branches are also indicated in figure 14, with solid lines indicating solutions which are stable (to one-dimensional disturbances) and broken lines indicating unstable solutions.

Our analysis described in the earlier subsections focused exclusively on the stability of solutions to disturbances for which ν and θ were symmetric about the centreline. When this restriction is imposed, the primary symmetric branches (see figure 4 corresponding to the same set of parameters as figure 14) were found to be linearly stable. Now, when we remove this restriction and allow asymmetric disturbances, the same primary branches are no longer linearly stable (compare figures 4 and 14).

Figure 15 shows the structure of a fully developed solution at point W in the primary asymmetric branch in figure 14. Panel (*a*) reveals that the ν-structure has a high density of particles near one wall and a low density of particles near the other. The corresponding dimensionless temperature and axial velocity profiles are shown in panels (*b*) and (*c*) respectively. As expected, the granular temperature is low in the region with high ν and vice versa. The region with high ν behaves essentially like a plug and shearing is limited almost completely to the dilute region. In the case of adiabatic walls, the relationship between the symmetric and asymmetric solutions can easily be recognized: by properly stacking the two asymmetric solutions corresponding to a given value of C, one can generate the symmetric solutions at $C/2$.

Figure 16 shows the bifurcation diagram for the parameter values in figure 14, except that the walls are now non-adiabatic. We see that for both source and sink

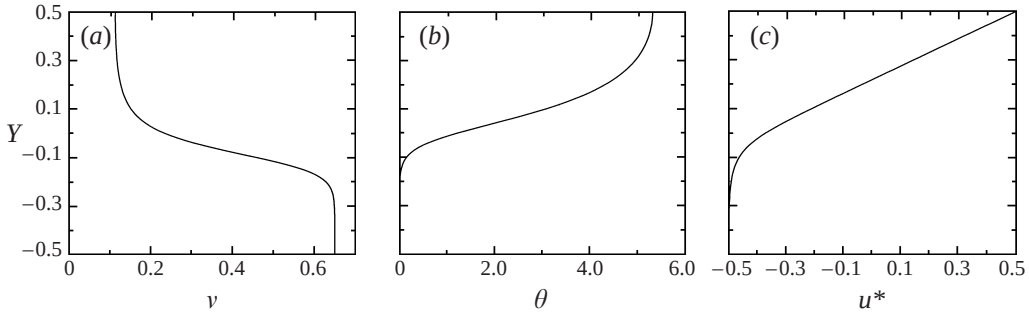

FIGURE 15. The structure of a fully developed asymmetric solution corresponding to point W in figure 14. $\bar{\nu} = 0.35$; $e_p = 0.8$; $C = 0.06$. (*a*) Particle volume fraction; (*b*) dimensionless temperature; (*c*) dimensionless axial velocity.

walls (panels *a* and *b* respectively), the characteristics of the bifurcation diagram are essentially the same as those for the symmetric case. The first asymmetric branch is the only stable branch, and it emerges from the primary symmetric branch (labelled branch 1 in figures 11 and 12). Additional asymmetric branches, all of which are unstable, originate from the limit points of the other symmetric branches.

5. Summary

We have presented a bifurcation analysis for steady fully developed plane Couette flow of a granular material, using the continuum equations of motion and a constitutive model appropriate for rapid shear. Our analysis gives the final steady states of the layering instabilities that were reported by Wang *et al.* (1996) and Alam & Nott (1998), and the stability of these branches in turn to layering disturbances. As in these earlier studies, we have studied the effect of wall properties by considering three representative sets of parameters that correspond to the walls being adiabatic, and sources and sinks of pseudo-thermal energy. The bifurcation diagram for a given set of grain and wall properties and the mean solids fraction $\bar{\nu}$ is given as a plot of the solids fraction at the centre, $\nu(0)$, versus the dimensionless inverse Couette gap C.

When the walls are adiabatic, the primary solution branch is that of uniform shear and constant density across the gap. As the Couette gap increases, bifurcations occur on this branch at equal intervals of $1/C$, and points on the bifurcating branches represent solutions with considerable non-uniformity in density and shear rate. Two types of non-uniform solutions, one with a dense region of particles in the centre and leaner regions near the wall, and another with a leaner region of particles in the centre and denser region near the walls, are both possible.

The bifurcations are supercritical when $\bar{\nu}$ is large, and become subcritical as $\bar{\nu}$ decreases. The value of C at each bifurcation point decreases with $\bar{\nu}$, and eventually when $\bar{\nu}$ falls below a critical value of roughly 0.156 the bifurcations occur at $C = 0$ (or infinite Couette gap). These 'bifurcations from infinity' imply that at low mean density there is a non-uniform solution coexisting with that of uniform shear for a range of C, even though the latter is linearly stable; this result explains the observation of segregated structures in the computer simulations of Tan (1995) at a low mean density. We have also presented transient simulations of the time-dependent equations of motion, which clearly show that the non-uniform solutions at low densities may be attained via finite-amplitude perturbations from the uniform shear solution. Our

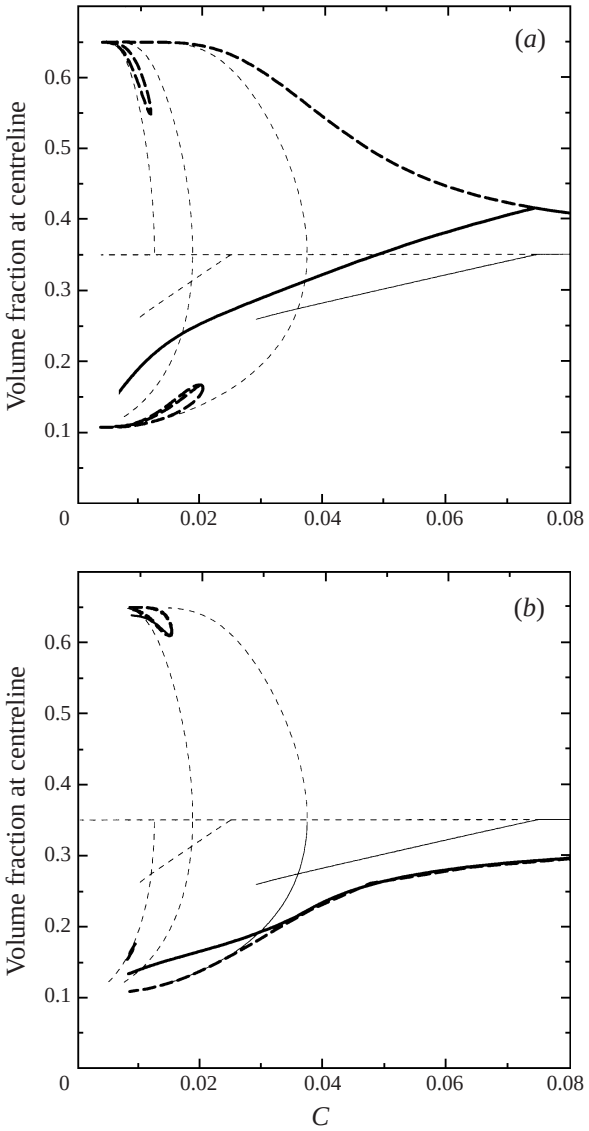

FIGURE 16. Bifurcation diagram showing both symmetric and asymmetric branches. Results are shown for $\epsilon = 0$ (thin lines) and $\epsilon = 1.0$ (thick lines). $\overline{\nu} = 0.35$; $e_p = 0.8$. (*a*) $e_w = 1.0$. (*b*) $e_w = 0.5$.

transient simulations also capture the coalescence of dense layers that was reported by Tan.

The effects of inelastic collisions and partial slip at the walls are then investigated by treating the extent of non-adiabaticity as a parameter. It is found that the role of the boundary is in selecting the primary branch; the primary branch represents solutions with a dense layer at the centre when the walls are energy sources, and dense layers near the walls when the walls are energy sinks. This result clearly demonstrates that there is no nearly uniform solution for non-adiabatic walls (except when C is large), and therefore that the base states found by Wang *et al.* (1996) for non-adiabatic walls are numerical artifacts.

This paper demonstrates that one-dimensional non-uniform structures found in

dynamic simulations of granular flow can be explained by the continuum equations of motion. Strictly speaking, the model developed by Lun *et al.* (1984) is valid only when the collisions between particles are nearly elastic. When this model is used in conjunction with solid boundaries, the particle–wall collisions should also be nearly elastic. Thus, our results for highly inelastic particles, such as the marginal stability contours for low e_p values in figure 2, should be regarded as qualitative.

Although the present work has been devoted to non-uniform solutions having only lateral structures, particle dynamics simulations reveal that a richer variety of solutions is possible when one allows both axial and lateral structures to develop simultaneously (Tan & Goldhirsch 1997). Stability analyses of the continuum equations (Wang *et al.* 1996; Alam & Nott 1998) do suggest the possibility stationary and travelling modes having both axial and lateral structure; a thorough exploration of the fate of these modes remains unexplored. It would be interesting to examine if two- and three-dimensional transient simulations of the continuum equations reveal features such as cluster–cluster interaction and churn flow reported by Tan & Goldhirsch (1997).

This work was supported by the National Science Foundation (CTS-9421661), the Exxon Education Foundation, and the International Fine Particle Research Institute.

Appendix. Bifurcation from infinity

Consider the eigenvalues of equations (4)–(7), linearized about the uniform base state. As shown in Alam & Nott (1998), the eigenvectors for this case are

$$\left.\begin{aligned} \hat{v}(y) &= \hat{v}_1 \cos k_n(y \pm \tfrac{1}{2}), \\ \hat{\theta}(y) &= \hat{\theta}_1 \cos k_n(y \pm \tfrac{1}{2}), \\ \hat{u}(y) &= \hat{u}_1 \sin k_n(y \pm \tfrac{1}{2}), \\ \hat{v}(y) &= \hat{v}_1 \sin k_n(y \pm \tfrac{1}{2}), \end{aligned}\right\} \tag{A 1}$$

where $k_n = n\pi$, n being a positive integer. Substituting (A 1) into the linearized governing equations yields the dispersion relation

$$\omega^4 + a_3\omega^3 + a_2\omega^2 + a_1\omega + a_0 = 0. \tag{A 2}$$

The coefficients a_0–a_3 are all real and depend on the mean volume fraction $\overline{\nu}$, the dimensionless functions of the volume fraction f_1–f_8, and k_n. The expressions are too cumbersome to reproduce here, but may be found in Alam (1998).

Two roots of (A 2) are real and the others form a complex-conjugate pair. In the limit of small C, the real roots have the form

$$\omega^{(1)} = -C^2\left(a_{04}/a_{12}\right) + O\left(C^4\right),$$

$$\omega^{(2)} = \omega_0^{(2)} + O\left(C^2\right),$$

with

$$\omega_0^{(2)} = -\frac{2}{3\overline{\nu}}(f_2 f_5)^{1/2} < 0,$$

and the real and imaginary parts of the conjugate pair are

$$\omega_r = C^2 \left(\frac{a_{04} + a_{12}^2/a_{30}^2 - a_{12}a_{22}/a_{30}}{2a_{12}} \right) + O\left(C^4\right)$$

$$\omega_i^2 = C^2 \left(a_{12}/a_{30}\right) + O\left(C^4\right).$$

The coefficients a_{ij} are independent of C (Alam 1998). It can be shown that ω_r is always negative, and that $\omega^{(1)}$ is the least-stable mode (Alam 1998); it is positive above a critical value $\bar{\nu}_*$ of the volume fraction, which is roughly 0.156 when $e_p = 0.8$, and negative below.

For $\bar{\nu} < \bar{\nu}_*$, it is clear from the above that the leading eigenvalue is negative, but decays to zero as C^2 when $C \to 0$. This falls under the class of problems described by Rosenblat & Davis (1979), which exhibit bifurcation from infinity. The essence of their result is as follows: a class of differential equations that yield a linearly stable trivial solution (in our case, that of uniform shear) for all finite values of a parameter, say μ, also yield solution(s) of finite norm (i.e. a finite distance away in phase space from the trivial solution) for large values of μ. The structure of this solution is qualitatively different from the eigenfunctions of the equations linearized about the trivial solution. Rosenblat & Davis show this behaviour for a variety of equations whose common characteristic is that the leading eigenvalue of the linearized equations decays to zero as $\mu \to \infty$. The non-trivial solution tends arbitrarily close (in phase space) to the trivial solution as $\mu \to \infty$, but grows apart from it as μ decreases. Moreover, this branch of solutions does not exist for small μ, but exhibits a limit point at some finite value of μ. Lastly, the branch of the non-trivial solution that is closer to the trivial solution is linearly unstable, while the one farther away is stable.

These characteristics are exhibited by the system of equations (4)–(7) when $\bar{\nu} < \bar{\nu}_*$, with the parameter μ identified as C^{-1}. Thus, it is reasonable to expect that the branch representing non-uniform solutions in figure 6(f) bifurcates from the uniform solution branch at $C = 0$.

REFERENCES

Agrawal, K. 1999 PhD Dissertation, in preparation, Princeton University.

Alam, M. 1998 Stability of unbounded and bounded granular shear flows. PhD Dissertation, Indian Institute of Science, Bangalore, India.

Alam, M. & Nott, P. R. 1998 Stability of plane Couette flow of a granular material. *J. Fluid Mech.* **377**, 99–136.

Babić, M. 1993 On the stability of rapid granular flows. *J. Fluid Mech.* **254**, 127–150.

Canuto, C., Hussaini, M. Y., Quarteroni, A. & Zang, T. A. 1988 *Spectral Methods in Fluid Dynamics*. Springer.

Doedel, E., Keller, H. & Kernevez, J. 1991 Numerical Analysis and control of bifurcation problems. I: Bifurcation in finite dimensions. *Intl J. Bifurcation Chaos* **1**, 493–520.

Goldhirsch, I., Tan, M.-L. & Zanetti, G. 1993 A molecular dynamical study of granular fluids I: the unforced granular gas in two dimensions. *J. Sci. Comput.* **8**, 1–40.

Hopkins, M. A. & Louge, M. Y. 1991 Inelastic microstructure in rapid granular flows of smooth disks. *Phys. Fluids* A **3**, 47–57.

Hui, K., Haff, P. K., Ungar, J. E. & Jackson, R. 1984 Boundary conditions for high-shear grain flows. *J. Fluid Mech.* **145**, 223–233.

Jenkins, J. T. & Louge, M. Y. 1997 On the flux of fluctuation energy in a collisional grain flow at a flat, frictional wall. *Phys. Fluids* **9**, 2835–2840.

Jenkins, J. T. & Richman, M. W. 1985*a* Grad's 13-moment system for a dense gas of inelastic spheres. *Arch. Rat. Mech. Anal.* **87**, 355–377.

Jenkins, J. T. & Richman, M. W. 1985*b* Kinetic theory for plane flows of a dense gas of identical, rough, inelastic, circular disks. *Phys. Fluids* **28**, 3485–3494.

Jenkins, J. T. & Richman, M. W. 1986 Boundary conditions for plane flows of smooth, nearly elastic, circular disks. *J. Fluid Mech.* **171**, 53–69.

Jenkins, J. T. & Savage, S. B. 1983 A theory for the rapid flow of identical, smooth, nearly elastic particles. *J. Fluid Mech.* **130**, 187–202.

Johnson, P. C. & Jackson, R. 1987 Frictional-collisional constitutive relations for granular materials, with applications to plane shearing. *J. Fluid Mech.* **176**, 67–93.

Louge, M. Y. 1994 Computer simulations of rapid granular flows of spheres interacting with a flat, frictional boundary. *Phys. Fluids* **6**, 2253–2269.

Lun, C. K. K. 1991 Kinetic theory for granular flow of dense, slightly inelastic, slightly rough spheres. *J. Fluid Mech.* **233**, 539–559.

Lun, C. K. K. & Savage, S. B. 1987 A simple kinetic theory for granular flow of rough, inelastic, spherical particles. *Trans. ASME* E: *J. Appl. Mech.* **54**, 47–53.

Lun, C. K. K., Savage, S. B., Jeffrey, D. J. & Chepurniy, N. 1984 Kinetic theories for granular flow; inelastic particles in Couette flow and slightly inelastic particles in a general flow field. *J. Fluid Mech.* **140**, 223–256.

McNamara, S. 1993 Hydrodynamic modes of a uniform granular medium. *Phys. Fluids* A **5**, 3056–3070.

Mello, T. M., Diamond, P. H. & Levine, H. 1991 Hydrodynamic modes of a granular shear flow. *Phys. Fluids* A **3**, 2067–2075.

Miller, T. M., O'Hern, C. & Behringer, R. P. 1996 Stress fluctuations for continuously sheared granular materials. *Phys. Rev. Lett.* **77**, 3110–3113.

Reddy, J. N. 1984 *An Introduction to the Finite Element Method.* McGraw-Hill.

Richman, M. W. 1988 Boundary conditions based upon a modified Maxwellian velocity distribution for flows of identical, smooth, nearly elastic spheres. *Acta Mechanica* **75**, 227–240.

Rosenblat, S. & Davis, S. H. 1979 Bifurcation from infinity. *SIAM J. Appl. Maths* **37**, 1–19.

Savage, S. B. 1992*a* Numerical simulations of Couette flow of granular materials: spatio-temporal coherence and 1/f noise. In *Physics of Granular Media* (ed. D. Bideau & J. Dodds), pp. 343–362. New York: Nova Science.

Savage, S. B. 1992*b* Instability of unbounded uniform granular shear flow. *J. Fluid Mech.* **241**, 109–123.

Schmid, P. J. & Kytömaa, H. K. 1994 Transient and asymptotic stability of granular shear flow. *J. Fluid Mech.* **264**, 255–275.

Strogatz, S. H. 1994 *Nonlinear Dynamics and Chaos: With Applications to Physics, Biology, Chemistry, and Engineering.* Addison-Wesley.

Tan, M.-L. 1995 Microstructures and macrostructures in rapid granular flows. PhD Dissertation, Princeton University, Princeton, NJ.

Tan, M.-L. & Goldhirsch, I. 1997 Intercluster interactions in rapid granular shear flows. *Phys. Fluids* **9**, 856–869.

Wang, C.-H., Jackson, R. & Sundaresan, S. 1996 Stability of bounded rapid shear flows of a granular material. *J. Fluid Mech.* **308**, 31–62.